



Identification of transparent and specular reflective material in laser scans to discriminate affected measurements for faultless robotic SLAM

Rainer Koch^{a,*}, Stefan May^a, Patrick Murmann^a, Andreas Nüchter^b

^a Technische Hochschule Georg-Simon-Ohm, Kesselerplatz 12, 90489 Nürnberg, Germany

^b Informatics VII – Robotics and Telematics, Julius-Maximilians University, Am Hubland, 97074 Würzburg, Germany

HIGHLIGHTS

- The need for discrimination between specular reflective and transparent objects for environmental mapping is demonstrated.
- The characteristics identified in the measurements of different objects based on distance, angle, and material are investigated.
- It is shown that shiny metallic materials provide significant characteristics, while mirrors are to be characterized by a mixed model (between glass and shiny metal).
- Mapping transparent objects turned out to be challenging because of the dependency on the object behind the surface.
- The problem of mapping transparent and specular reflective objects is treated with an extended version of the Mirror Detector Approach, named Reflection Classifier Approach. It demonstrates the solvability of this problem.

ARTICLE INFO

Article history:

Received 4 December 2015

Accepted 17 October 2016

Available online 29 October 2016

Keywords:

SLAM

Error-free mapping

Multi-echo laser scanner

Reflectance filter

Specular reflection

Reflective objects

Material discrimination

ABSTRACT

Mapping with laser scanners is the state-of-the-art method applied in service, industrial, medical, and rescue robotics. Although a lot of research has been done, maps still suffer from interferences caused by transparent and specular reflective objects. Glass, mirrors, shiny or translucent surfaces cause erroneous measurements depending on the incident angle of the laser beam. In past experiments the Mirror Detector Approach was implemented to determine such measurements with a multi-echo laser scanner. Recognition values are based on their differences in recorded measurements in regard to the distance of the echoes. This paper describes the research to distinguish between reflective and transparent objects. The implemented Mirror Detector was specifically modified for recognition of said objects for which four experiments were conducted; one experiment to show the map of the original Mirror Detector; two experiments to investigate intensity characteristics based on angle, distance, and material; and one experiment to show an applied discrimination with the extended version of the Mirror Detector, the Reflection Classifier Approach. To verify the results, a comparison with existing models was performed. This study showed that shiny metals, like aluminium, etc., provide significant characteristics, while mirrors are to be characterized by a mixed model of glass and shiny metal. Transparent objects turned out to be challenging because their appearance in the sensor data strongly depends on the background. Nevertheless, these experiments show that discrimination of transparent and reflective materials based on the reflected intensity is possible and feasible.

© 2016 Elsevier B.V. All rights reserved.

1. Introduction

In mobile robotics, mapping is an essential task. In service robotics, industrial, medical, and rescue applications the environment is partly or completely unknown before starting a mission [1]. Simultaneous Localization and Mapping (SLAM) is one

of the most frequently applied approaches for providing an environmental representation for mobile robots. Therefore, robots are often equipped with a laser scanner to supply accurate distance measurements. One drawback to laser scanners is their sensitivity to specular reflective and translucent surfaces, e.g., glass, mirrors, or shiny metal. When scanning such a surface, the laser beam can provide misleading measurements (see Fig. 1).

Glass surfaces are reflective or transparent depending on the incident angle of the laser beam. Objects behind the glass surface

* Corresponding author.

E-mail address: rainer.koch@th-nuernberg.de (R. Koch).



Fig. 1. Robot equipped with laser scanner facing an unframed mirror.

are only occasionally visible. Even worse is the aspect that the glass surface is registered as a volatile (disappearing) object or as not being visible at all. This carries the risk of crashing a robot into such surfaces. Mirrors and shiny metal redirect the laser beams. Therefore, at certain positions, phantom-like objects appear in the map. Hence, customizing most environments is necessary to reduce interferences from such objects. One way to handle these situations is to rely on a second sensor principle, like ultrasonic arrays. This adds additional complexity to the application. In a preceding study, we had introduced the Mirror Detector for multi-echo laser scanners [2] based exclusively on the distance and intensity information provided.

Fig. 2 depicts the effects of reflective objects for three state-of-the-art SLAM approaches using the same dataset: Critical Rays Scan Match-SLAM (CRSM-SLAM) [3], Hector-SLAM [4] and Truncated Signed Distances-SLAM (TSD-SLAM) [5]. Furthermore, the TSD-SLAM combined with the Mirror Detector is shown. It is worth mentioning that the robot supports neither inertial measurements nor dead reckoning. Therefore, only mapping approaches are selected which do not require them.

The location of the mirror is marked by a blue rectangle and magnified on the top left. Phantom-like objects are marked by the red broken line rectangle. Hector-SLAM creates a static map, i.e., points added once to the map remain ad infinitum. The mirror is partly recognizable in the Hector-SLAM map due to the fact that at some positions the laser beam is not deflected. In comparison, CRSM- and TSD-SLAM build a dynamic map. Changes in the environment are considered in both approaches, e.g., when objects are moved. Therefore, the mirror disappears if its surface is not measurable at certain perspective views. This is likely the case when passing by a mirror. The map of the TSD-SLAM with the Mirror Detector does not show any phantom-like objects, but it contains the reflective object (mirror). In [2] we have pointed out the importance of distinguishing between transparent and specular reflections to improve map quality.

In the following, we present research to distinguish between specular reflective and transparent objects using multi-echo laser scanners in order to classify the effects mentioned above. Section 2 outlines related work. Section 3 describes the basic function of the Mirror Detector as it is used to record the data. In Section 4, one experiment shows the resulting map of the Mirror Detector. Then two experiments demonstrate the applicability to differentiate various specular reflective and transparent materials based on the intensity of the returning echoes of the laser beam. Experiment 4 shows an applied discrimination for translucent and specular reflective objects using an extended Mirror Detector approach, further called Reflection Classifier. In the end, Section 5 summarizes results and offers an outlook for future work.

2. Related work

As far as reflections are concerned, there are two different branches of research – stationary and mobile systems. When working with stationary systems, the environment is often adapted to prevent influences. This is difficult when working with mobile systems, since the area is often unknown or changes. Therefore, specular reflective surfaces might be covered manually under certain circumstances. An approach also capable of dealing with reflective phenomena is preferable since it reduces preparation efforts. Besides, it is applicable in unknown environments.

To avoid the need to cover surfaces for mapping, several approaches describe sensor fusion algorithms to distinguish discrepancies. To detect reflections, Yang et al. [6] fused a laser scanner with an ultrasonic sensor. Based on differences in the two individual grid maps, a discrimination of reflections was done. Later he and his team extended the algorithm to identify mirrored images [7]. This version assumes every gap in laser lines resulting from reflective objects. Therefore, no ultrasonic sensor is further required. Once a potential mirror is detected, the space behind the gap was analysed for a mirrored image, i.e., the search for similarities between both sides of the opening was conducted. Objects with symmetry w.r.t. a line could likely be identified incorrectly. Additionally, the discrimination between a reflection caused by a transparent or a specular reflective object was not discussed in Yang's study.

Another applicable online approach was implemented by Forster et al. [8]. At specific angles, reflections were identified based on the returning intensity of the laser. A subset of these angles was tracked – on occurrence mirrors were assigned according to the laser beam's intensity. An object with diffuse reflectivity caused false identification when it was placed directly behind the transparent object.

Tatogulu et al. [9] used the most suitable illumination model to modulate the surface. Lambertian diffuse reflection models, Blinn-Phong models [10], Gaussian models [11] and Beckmann specular reflection models [12] were matched to the data set to identify the characteristics of the scanned surface. While this system is quite effective for diffuse surfaces, it does not however, cover specular reflections.

Also, Yoshitaka et al. [13,14] used intensity values to improve the mapping of the environment containing interfering objects. The algorithm assumes that smoothness in intensity is related to smoothness in distance. Therefore, a conventional Iterative-Closest-Point algorithm (ICP [15]) was combined with an intensity ICP to achieve an accurate position. Nonetheless, the approach does not use the intensity to ascertain any material.

None of the mentioned approaches use the intensity values to distinguish between specular reflective and transparent reflective surfaces. In previous work, we presented the Mirror Detector Approach to identify reflections based on differences in the laser scan echoes [2]. The related distance values of the two echoes were compared and analysed. The need to distinguish reflection behaviours, e.g., to distinguish between a reflection of a mirror or an object behind a transparent object, is pointed out in the conclusion section of [2]. In this work the experimenters present research to identify different transparent and specular reflective materials according to their intensity characteristics based on the Mirror Detector Approach. Further, the improvement in SLAM was pointed out with the Reflection Classifier Approach.

3. The Mirror Detector approach

The Mirror Detector was used to record the data for the Experiments 1, 2, and 3 in Section 4. Additionally, it was extended in Experiment 4, by a function to ascertain specular reflective

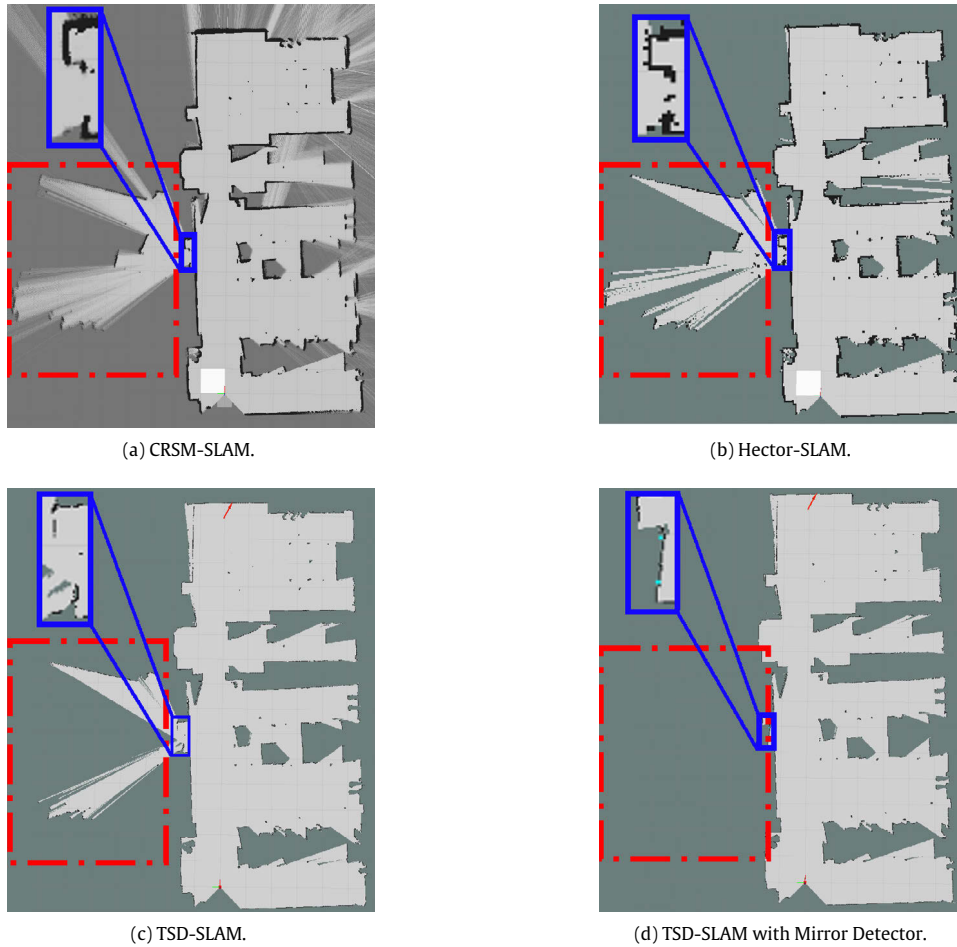


Fig. 2. Maps registered from the same dataset with different SLAM approaches in an environment containing a mirror. The mirror is marked by a blue solid line, reflections are marked by a red broken line.

and transparent objects. Section 3.1 describes the Mirror Detector as it is presented in [2] to give the reader required background information. Section 3.2 describes the applied modifications and the used values for the experiments in the preceding section.

3.1. Mirror Detector approach

The Mirror Detector uses a Hokuyo 30LX-EW multi-echo laser scanner and the TSD-SLAM module [5]. For each data taken the Hokuyo records up to three echoes of the returning light wave, including distance and intensity. Differences in scan messages indicate surface reflection properties. While a specular reflective object causes strong differences in both scan messages, diffuse reflective objects provide near consistency. The problem in detecting specular reflections is that it depends both on the laser beam's incident angle to the surface and the refractive index. If the angle is too large, the light will be completely reflected. Subsequently, the robot will only detect the mirrored object and, if the angle is smaller, there are up to three potential cases of measurements. For a transparent object, the robot can receive a point on the surface, a point behind the surface, or a mirrored point. If the object is non-transparent, the second case does not apply. As a result of the incident angle dependency, the robot has to pass the surface to ensure that it was seen at least once from the "right" perspective. If so, the reflective object is identified and reflective errors subsequently removed. Hence, it is not possible to eliminate all reflective errors instantaneously. Because of this, the Mirror Detector is set up in two filter stages, a pre- and a post-filter.

Both stages are connected to a mapping module, e.g., TSD-SLAM, cf. Fig. 3.

Pre-filter processing runs on the fly and filters current scans. It filters scan points only if the incident angle is in the required range. Fig. 3a shows the processing chain of the pre-filter with its mapping stage. Reflection errors, which are detectable in a single data take, are removed. Hence, the map includes less erroneous data than a map which has received raw data. Since not all reflections are detectable in a single scan, the map is not completely free from reflective influences. Thus, pre-filtered scans and detected reflective points are passed to the post-filter.

The post-filter, cf. Fig. 3b, builds up a history of these scans, the detected reflective points and the robot poses. The history is used to merge measurements from different perspective views. This increases the probability of identifying specular reflective areas. The mapping stage assigned to the post-filter chain considers a set of scan tuples. All measurements are preprocessed which results in the elimination of reflective influences. This supplies a map free of any reflection errors available at new trigger events, e.g., from a loop closure module. All modules are implemented as ROS-nodes and are publicly available as open-source packages at: http://www.github.com/autonohm/ohm_mirror_detector.git.

3.1.1. Pre-filter:

The pre-filter, see Algorithm 1, receives a scan tuple with N representing scan points

$$S = \{s_{1,i}, s_{2,i} \mid i = 1, \dots, N\},$$

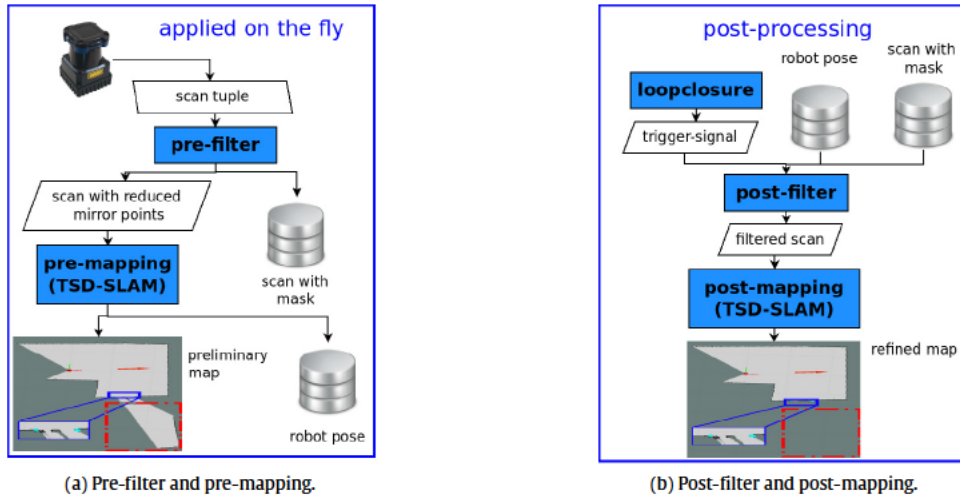


Fig. 3. Processing chains of the Mirror Detector: Pre-filtering removes affections on the fly. Post-filtering refines the resulting map after a trigger signal. The differences of both maps are highlighted at the bottom side.

the corresponding angles

$$\alpha = \{\alpha_{1,i}, \alpha_{2,i} \mid i = 1, \dots, N\},$$

and the corresponding intensities

$$I = \{int_{1,i}, int_{2,i} \mid i = 1, \dots, N\}$$

from the laser scanner. It removes sparse points from the scan tuple S in a first step

$$D = \{d_{1,i}, d_{2,i} \mid i = 1, \dots, N\}.$$

These isolated points without other points nearby are likely to be artefacts, for example from jumping edges. They appear when neighbouring measurements cross an object edge and provide discontinuity in depth. Further, the corresponding points in the scan tuple are subtracted. A difference between two scan tuples indicates that the laser beam is specularly reflected. The threshold γ is used to identify a mismatch, which happens when the laser beam hits a reflective or transparent surface. It is generally known that the first echo $d_{1,i}$ originates from the reflective/transparent object, since it was hit first by the laser beam. The second echo $d_{2,i}$ includes a point further away, henceforth called the affected point. As a result, the function *identifyReflection()* returns three groups of points:

$$\begin{cases} d_{1,i} \leftarrow G_{\text{valid},i}, & \text{if } \Delta d_i \leq \gamma \\ d_{1,i} \leftarrow G_{\text{mirror},i}, \quad d_{2,i} \leftarrow G_{\text{affected},i}, & \text{if } \Delta d_i > \gamma \end{cases} \quad (1)$$

with

$$\Delta d_i = d_{2,i} - d_{1,i}. \quad (2)$$

Glass fronts and mirrors are assumed to be planar. Therefore, a line with two end points is sufficient to model the surface. A RANSAC-based algorithm determines these end points \vec{c}_1 and \vec{c}_2 out of the mirror group, cf. Fig. 4. This only applies, if enough points are located on the surface.

With robot position \vec{p} , end points \vec{c}_1 and \vec{c}_2 a sector $\alpha_{(\vec{c}_1, \vec{c}_2)}$ is spanned up. Dirt on the object and roughness of its surface may result in an incorrect identification in the first step. For this reason, the scan is checked again to remove outliers. Each point of the scan g_i , which is located between the corners \vec{c}_1 and \vec{c}_2 , is projected onto the mirror plane to obtain the related point c_i on the mirror plane. The difference of g_i and c_i determines whether g_i is placed in front of, on, or behind the mirror or transparent object. In order to take disturbances in measurement into account, threshold ϵ

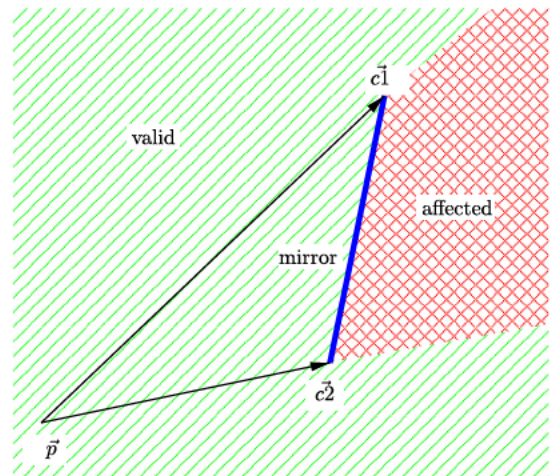


Fig. 4. Classification of points based on the mirror line corners. (For interpretation of the references to colour in this figure legend, the reader is referred to the web version of this article.)

is designated to define the blue area around the mirror plane. ϵ depends on the accuracy of the laser scanner. “Valid” points are located in the green hatched area in front of the mirror. They are free of any reflection influences. The second group, “mirror”, contains points on mirrors, windowplanes, and reflective metallic surfaces. They are found in the solid blue area. All remaining points can be found in the red crossed area behind the plane and are assigned to the third group, henceforth called “affected” points.

3.1.2. Post-filter:

The post-filter, see Algorithm 1, receives a masked scan tuple

$$S_1 = \{s_{1,i}, s_{2,i}, \alpha_i, int_{1,i}, int_{2,i}, m_i \mid i = 1, \dots, N\}$$

from the pre-filter, where s_1 are the scan points of Echo 1, s_2 are the scan points of Echo 2, α is the scanning angle, int_1 the intensities of Echo 1, int_2 the intensities of Echo 2, m a mask for valid points, and N is the amount of points per scan.

It requests the transformation matrix T from the ROS-TF-node. This module supports all positions for certain timestamps. The transformation is used to convert the scan tuple S_1 (in the robot coordinate system) into a scan tuple S_2 (in the world coordinate system). Subsequently, all points which were masked as “mirror”

Algorithm 1 Pre-filter1**Input:** S, α, I :

S includes the scan points of Echo 1 and Echo 2, α includes the corresponding angles, and I includes the corresponding intensities of Echo 1 and Echo 2. N is the amount of scan points per echo.

Output: $G_{2,\text{valid,mirror,affected}}$:

$G_{2,\text{valid}}$ includes the valid scan points with their corresponding intensities, $G_{2,\text{mirror}}$ includes the scan points, located on the surface of the transparent or specular reflective object, with their corresponding intensities, and $G_{2,\text{affected}}$ includes the scan points, located behind the surface of the transparent or specular reflective object, with their corresponding intensities.

```

1: procedure PREFILTER
2:    $S, \alpha \leftarrow \text{receiveScanTuple}()$ 
3:    $D \leftarrow \text{removeSparsePoints}(S)$ 
4:    $G_{1,\{\text{valid,mirror,affected}\}} \leftarrow \text{identifyReflection}(D, I, \alpha)$ 
5:    $(\vec{c}_1, \vec{c}_2) \leftarrow \text{findLine}(G_{1,\text{mirror}})$   $\triangleright$  get corners of line
6:    $(\alpha_{\vec{c}_1}, \alpha_{\vec{c}_2}) \leftarrow \text{spanUpAngles}(\vec{c}_1, \vec{p}, \vec{c}_2)$ 
7:   for  $i = 0, i < N, i++$  do  $\triangleright$  resort outliers, cf. Figure 4
8:      $G_{2,\text{valid},i}, G_{2,\text{mirror},i}, G_{2,\text{affected},i} \leftarrow 0$ 
9:      $d_{p,\text{mirror}} \leftarrow \|\vec{c}_i - \vec{p}\| - g_i$ 
10:    if  $\alpha_i < \alpha_{\vec{c}_1}$  &  $\alpha_i > \alpha_{\vec{c}_2}$  then
11:       $G_{2,\text{valid},i} \leftarrow g_i, I_i, \alpha_i$ 
12:    else
13:      if  $d_{p,\text{mirror}} < -\epsilon$  then
14:         $G_{2,\text{valid},i} \leftarrow g_i, I_i, \alpha_i$ 
15:      else if  $d_{p,\text{mirror}} > \epsilon$  then
16:         $G_{2,\text{affected},i} \leftarrow g_i, I_i, \alpha_i$ 
17:      else
18:         $G_{2,\text{mirror},i} \leftarrow g_i, I_i, \alpha_i$ 
19:      end if
20:    end if
21:  end for
22:   $\text{sendFilteredScans}(G_{2,\{\text{valid,mirror,affected}\}})$ 
23: end procedure

```

or “affected” are singled out into the groups $A_{1,\text{mirror}}$ and $A_{1,\text{affected}}$. Finally S_2 , and A_1^* are stored in a history bank G_1 .

$$G_1 = \{S_2, A_1, |j = 1, \dots, L\}$$

where L is the length of the history.

This procedure is repeated for every incoming scan. The post-filter is triggered after a reflective object was passed in order to reduce remaining errors, e.g., by a passing-algorithm or a loop-closure.

As soon as the post-filter has received the trigger signal, the function *findLine()* searches the entire history $G_{A1,\text{mirror}}$ for reflective objects. The function is based on the same RANSAC-based algorithm which was already used in the pre-filter. In contrast to the pre-filter, this time there are more scan points, since the post-filter does not rely on a single scan but on the entire history. The history contains scans from different positions. That is why the reflective object was seen from many different perspectives. Hence, it is assumed that each part of the object had been seen at least once. As a result the RANSAC of the post-filter creates a more accurate model compared to the pre-filter. The resulting end points \vec{c}_1 and \vec{c}_2 , of each object O , are used together with the position of the robot in order to span up a sector, similar as it is done at the pre-filter, c.f. Fig. 4. Subsequently, each scan point of the entire history is classified based on the “precise” reflective object model. The points masked as “valid”, “mirror”, or “affected” are stored in G_2 . The function *identifyReflectionType()* is an extension of the Mirror Detector Approach to distinguish between objects of different types. The function *identifyReflectionType()* was implemented

during the following experiments. This aspect is thus described in detail in Section 4.3.4.

Finally, five different scan messages are published. The first message is called “valid” and contains the points $G_{A2,\text{valid}}$, but also the points on the mirror plane $G_{A2,\text{mirror}}$; the points on the transparent plane $G_{A2,\text{transparent}}$; and the points behind the transparent plane $G_{A2,\text{transparent_affected}}$, because they represent real objects. In addition separate messages called “mirror”, “transparent”, “mirror_affected”, and “transparent_affected” are also published. The message “mirror” contains the points $G_{A2,\text{mirror}}$; the message “transparent” contains the points $G_{A2,\text{transparent}}$; the message “mirror_affected” contains the points $G_{A2,\text{mirror_affected}}$; and the message “transparent_affected” contains the points $G_{A2,\text{transparent_affected}}$. The points $G_{A2,\text{mirror_affected}}$ are not used yet, but it remains the aim of future work. These points are caused by objects mirrored on the specular reflective surface.

3.1.3. TSD-SLAM:

Exemplarily, the TSD-SLAM [16] software is used to verify the results of the Mirror Detector. TSD-SLAM uses depth measurements from arbitrary 2D/3D sensor units to build a map based on the signed distance function. The underlying framework generalizes the KinectFusion approach with an object-oriented model respecting different sensor modalities. For instance, measurements of 2D/3D laser range finders and RGB-D cameras are integrated into the same representation. The approach does not depend on additional pose information, e.g., supported by IMU or dead reckoning. Due to the low drift, the approach is a proper candidate for the experiments in this paper. It is worth mentioning that any other mapping algorithm is possible to use with the Mirror Detector as well as the Reflection Classifier. In this case, it is important to ensure the support of the robot pose to the post-filter module.

3.2. Modified Mirror Detector Approach for experiments

To record the data for the experiments, the pre-filter was customized. The distance and intensity values of both echoes were saved separately and were used as input for the research in this paper. The experimenters used a Hokuyo 30LX-EW with following specifications:

Hokuyo 30LX-EW:	
Scan points (N):	1080
Scan frequency:	50 Hz
Scan angle:	270°
Angular resolution:	0.25°
Wave length λ :	905 nm
Distance range (Echo 1 and Echo2):	0.1–60 m
Intensity range:	0–2 ²⁴ *

* The measured intensity during the experiments was <22000.

The variables of the pre-filter were set to:

Pre-filter:	
Subtract threshold (ϵ):	5 cm
Particle filter threshold	5 cm
RANSAC threshold	4 cm
RANSAC iterations	100 iterations
RANSAC points to fit model	20 points
Min. points on surface	40 points

The variables of the post-filter were set to:

Post-filter:	
Threshold around corner	15 cm
Threshold around mirror line (γ)	5 cm
Angle threshold	20°
RANSAC threshold	4 cm
RANSAC iterations	100 iterations
RANSAC points to fit model	40 points

Algorithm 2 post-filter**Input:** S :

S includes the scan points of Echo 1 and Echo 2, the corresponding intensities, angles are included along with an object mask according to the assignment of the pre-filter. N is the amount of scan points and L is the length of the history of received scans.

Output: $G_{A2,valid,mirror,transparent,mirror_affected,transparent_affected}$:

$G_{A2,valid}$ includes the valid scan points, $G_{A2,mirror}$ includes the scan points located on the surface of the specular reflective object, $G_{A2,transparent}$ includes the scan points located on the surface of the transparent object, $G_{2,mirror_affected}$ includes the scan points located behind the surface of the specular reflective object, and $G_{2,mirror_affected}$ includes the scan points located behind the surface of the specular reflective object.

```

1: procedure POSTFILTER
2:    $S_1 \leftarrow \text{receiveMaskScan}()$ 
3:    $T \leftarrow \text{requestTf}(\text{timestamp}_{Scan})$ 
4:    $S_2 \leftarrow \text{moveInWorldCoordinateSystem}(S_1, T)$ 
5:    $A_{1,\{mirror,affected\}} \leftarrow \text{extractCorrupted}(S_2)$ 
    $\triangleright$  points which are on the reflective object or corrupted by it
6:    $G_1 \leftarrow \text{storeHistories}(S_2, A_1, M)$ 
7:   if externalTrigger() then  $\triangleright$  e.g., external loopclosure
   detection
8:      $(\vec{c}_1, \vec{c}_2) \leftarrow \text{findLine}(G_{A1,mirror})$   $\triangleright$  get corners of lines
9:     for  $j = 0, j < L, j++$  do
10:      for  $i = 0, i < N, i++$  do  $\triangleright$  resort outliers, cf.
   Figure 4
11:        $G_{A2,valid,j,i}, G_{A2,mirror,j,i}, G_{A2,affected,j,i} \leftarrow 0$ 
12:        $d_{p,mirror} \leftarrow \|\vec{c}_{j,i} - \vec{p}\| - g_i$ 
13:       if  $\alpha_{j,i} < \alpha_{\vec{c}_1}$  &  $\alpha_{j,i} > \alpha_{\vec{c}_2}$  then
14:          $G_{A2,valid,j,i} \leftarrow g_{j,i}$ 
15:       else
16:         if  $d_{p,mirror} < -\epsilon$  then
17:            $G_{A2,valid,j,i} \leftarrow g_{j,i}$ 
18:         else if  $d_{p,mirror} > \epsilon$  then
19:            $G_{A2,affected,j,i} \leftarrow g_{j,i}$ 
20:         else
21:            $G_{A2,mirror,j,i} \leftarrow g_{j,i}$ 
22:         end if
23:       end if
24:     end for
25:      $G_{A3,*} \leftarrow \text{identifyReflectcionType}$ 
    $\triangleright$  * stands for valid, mirror, transparent, mirror_affected,
   transparent_affected
    $\triangleright$  cf. Algorithm 3 in Section 4.3.4 as an add on of the experi-
   ments
26:     sendFilteredScans( $G_{A3,*}$ )
27:   end for
28: end if
29: end procedure

```

4. Experiments and results

This chapter demonstrates four experiments to show the necessity and the realizability of object discrimination. Further, they show the improvement for SLAM. The first experiment used the Mirror Detector Approach to point out its drawbacks and the need of a discrimination of specular reflective and translucent objects.

Experiments 2 and 3 were made to identify proper reflection models for multi-echo laser scanners for different materials. Inspired by the work of Tatogulu et al. [9] the experimenters used the Phong reflection model [17] as a basis to analyse different materials. The second experiment was conducted to identify the reflection characteristics on surfaces in a static scene to compare

it with the Phong model. In Experiment 3 a mobile platform was used to show the reflection characteristics in a dynamic scenario. For this, the scanner was moved on a track along the sample. This is a realistic case when robots explore and map an environment.

In the final experiment, a map with the Reflection Classifier was made. It used the applied results of Experiments 2 and 3 and point out the improvement for SLAM.

4.1. Experiment 1: TSD-SLAM with Mirror Detector approach

This experiment used the Mirror Detector Approach. Fig. 5a shows a glass surface and Fig. 5b shows a mirror. Both were located at the mapped area. The maps, resulting from the scans of the preliminary SLAM module and refined SLAM module, are illustrated in Fig. 6. The glass surface is marked by a blue dotted rectangle while the mirror is marked by a blue solid rectangle. Both were magnified to illustrate the differences in the preliminary and the refined maps. The points behind the glass and the points reflected by the mirror are marked by a red broken line rectangle. In the resulting map of the post-filter, cf. Fig. 6b, both planes (mirror, glass) were visible and the points located behind the planes were removed. In the case of the mirror plane, these values were corrected properly. In the case of the glass plane, the correction of values was incorrect and was therefore deemed undesirable. Since these points illustrated an object behind the glass plane, the points had to remain. The following two experiments were used to build models to discriminate a reflective surface from a transparent surface to handle such situations.

4.2. Experiment 2: Static scene

To identify the parameters of the reflection model of different surfaces, Figs. 7a and 7b show the setup of the laser scanner as well as the sample mount, both of which were affixed to a track. Only scan points detected on the sample surface b ($b = 52$ cm) were recorded. The distance s between sample and laser scanner was extended in 0.5 m steps between $s = [0.5, 6.5]$ m. It is understood that the angular range shrinks with increasing distance. Therefore, the number of measurements on the sample decreased. To eliminate stochastic errors the arithmetic mean intensity I_{mean} of $L = 5000$ measurements was taken. This does not reduce systematic errors which remain, such as contamination of the sample surface, quantization errors, roughness of the surface and mechanical misalignments. These errors are slightly noticed in Fig. 11, e.g., in a peak that is not aligned exactly at 0° .

The experiment was conducted with glass ($w = 6$ mm), transparent plastic ($w = 4$ mm), a mirror, an aluminium plate, white paper, red paper, yellow paper, blue paper and green paper as shown in Fig. 7c.

4.2.1. Intensity characteristic related to the Phong reflection model

The Phong illumination model, also applied in this study, describes the measurable intensity of each point individually in dependency of the incident angle and surface properties. It comprises ambient, diffuse, and specular proportions:

$$I_{\text{out}} = I_{\text{ambient}} + I_{\text{diffuse}} + I_{\text{specular}}, \quad (3)$$

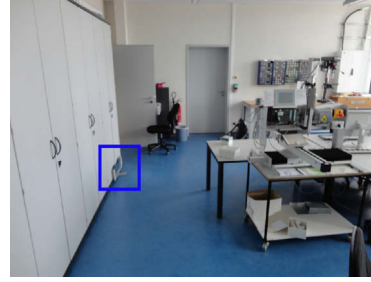
where I_{out} states the measured intensity.

We were interested in modelling the reflection of laser beams hitting surfaces with different properties. The measurable intensity of the returned laser beam was mainly caused by specular reflection. Hence, the modelling neglected ambient and diffuse proportions and focused only on the last term of Eq. (3).

$$I_{\text{specular}} = I_{\text{in}} \cdot k_{\text{specular}} \cdot \cos^n \theta, \quad (4)$$

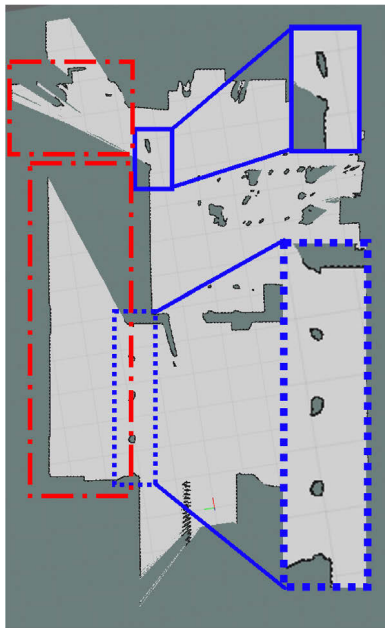


(a) Picture of area with glass surface.

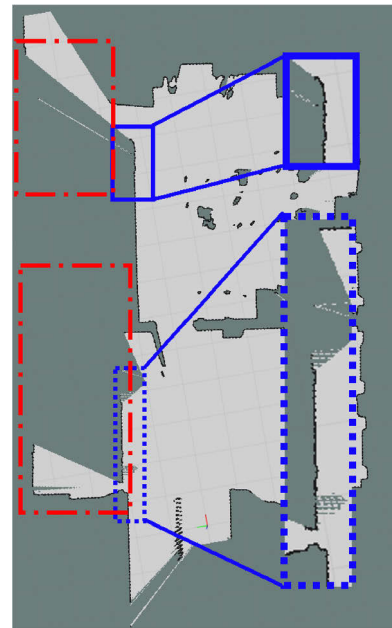


(b) Picture of area with mirror, marked by a blue solid rectangle in the map.

Fig. 5. Test area with a glass surface and a mirror from Experiment 1.



(a) Map created from the data of the pre-filter with TSD-SLAM.



(b) Map created from the data of the post-filter with TSD-SLAM.

Fig. 6. Maps created with the pre- and post-filter of the Mirror Detector Approach.

where I_{in} defines the intensity arriving at the surface, $k_{specular}$ is an empirically determined reflection factor, θ is the angle of incidence on the surface, and n is a factor to describe surface properties.

For diffuse surfaces, n is small. Higher values belong to specular reflective surfaces. An ideal mirror has $n = \infty$.

The normalized intensity returning from different surfaces is illustrated in Fig. 8.

Figs. 9–14 illustrate the intensity function for different distances and materials of Echo 1. The curves for paper with different colours do not show significant differences. An example with white paper and blue paper is illustrated in Figs. 9 and 10. Likewise, the intensity curve of aluminium, cf. Fig. 11, likens to be a Phong reflection curve with a high value for n . Therefore, the measurements were normalized, since the shape of the curve remains unchanged regardless of the distance. This is exemplarily illustrated in Fig. 15 with measurements of a white paper and an aluminium sample. Using $n = 5$ the Phong model describes best the curve of the white paper sample, while $n = 4000$ applies to the curve of the aluminium sample. It is not possible to describe the curve of glass, cf. Fig. 13, or transparent plastic, cf. Fig. 14, with this model. Instead, it seems that there is no dependency on the incident angle and the distance. They show many discontinuities.

Additionally, the maximum intensity values are significantly less than the corresponding values of paper or aluminium. This is due to the fact that the light is hardly reflected on the surface. Most of the light passed through the object, as was anticipated. The mirror is comprised of glass and a specular surface. Thus, an overlay of both effects was expected Fig. 12.

4.2.2. Intensity characteristic related to the distance

Apart from the dependency on the incident angle, the intensity also depends on the distance to the surface:

$$I_{received} \sim \frac{I_{sent}}{s^2}, \quad (5)$$

with s defining the distance between object and surface, $I_{received}$ is the received intensity of the scanner, and I_{sent} is the transmitted intensity of the scanner.

Figs. 16–19 illustrate this effect, which is especially noticeable for the paper surface and aluminium surface. It also confirms that glass has a high level of discontinuity. Moreover, it confirms that the mirror combines both effects measured from aluminium and glass.

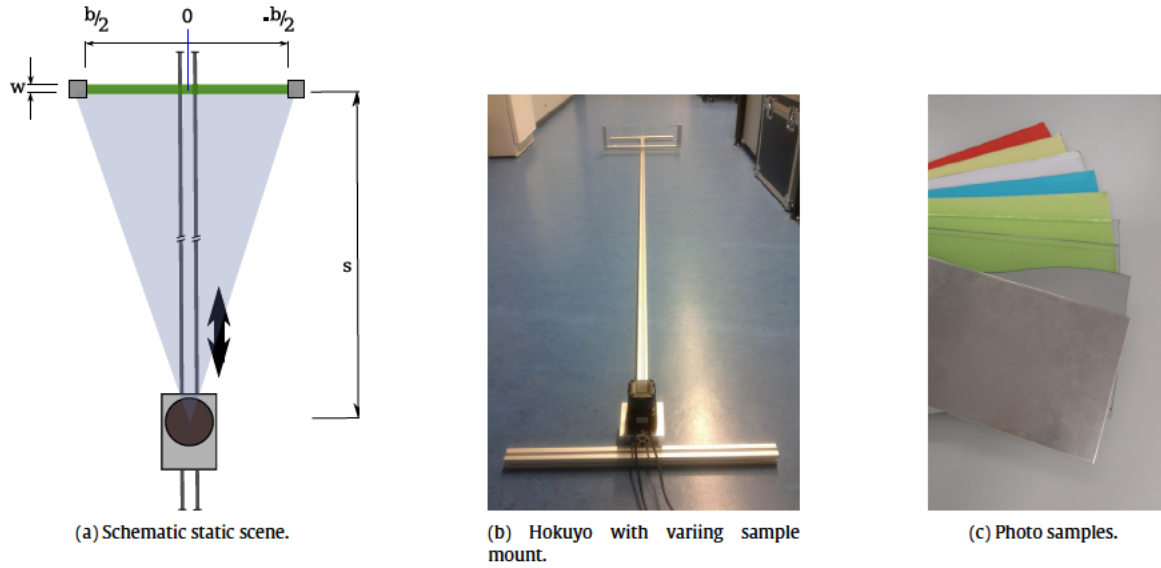


Fig. 7. Setup of Experiment 2. (For interpretation of the references to colour in this figure legend, the reader is referred to the web version of this article.)

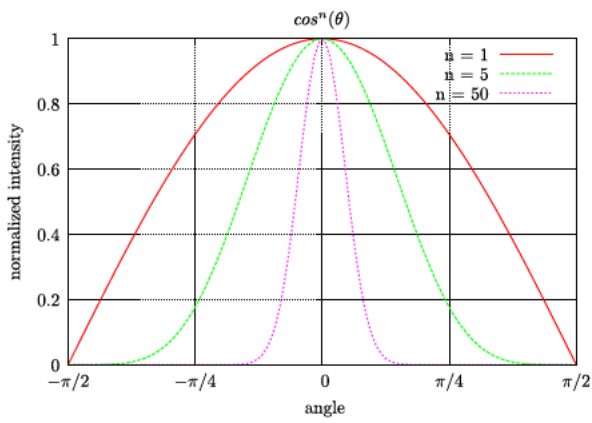


Fig. 8. Phong specular reflection curve [17].

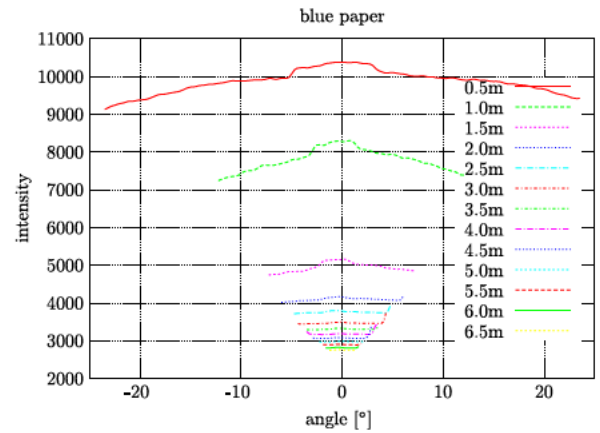


Fig. 10. Measured intensity curves returned from blue paper at different distances.

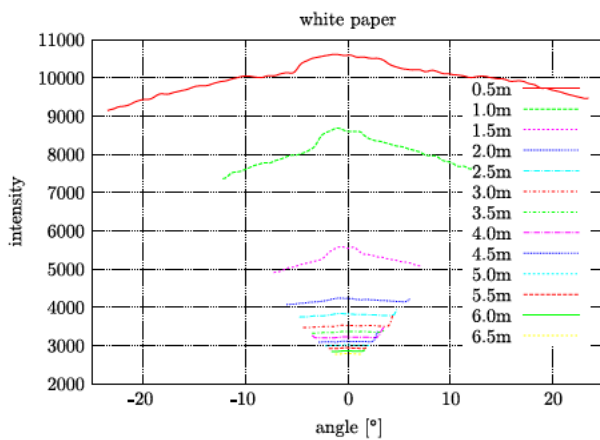


Fig. 9. Measured intensity curves returned from white paper at different distances.

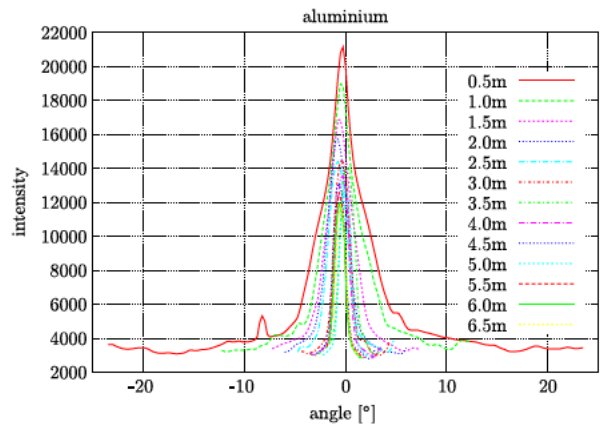


Fig. 11. Measured intensity curves returned from aluminium at different distances.

Fig. 20 illustrates the intensity via distance for a perpendicular incident angle. Five scan points around the angle were taken to build a mean value. Since only 12 distances were measured the

curve is a rough approximation. It is assumed that the first measurement at $s = 0.5$ m for the mirror is a mismatch. Otherwise results would have indicated that the intensity of the laser beam increased with an enlarging distance to the object. Since the beam

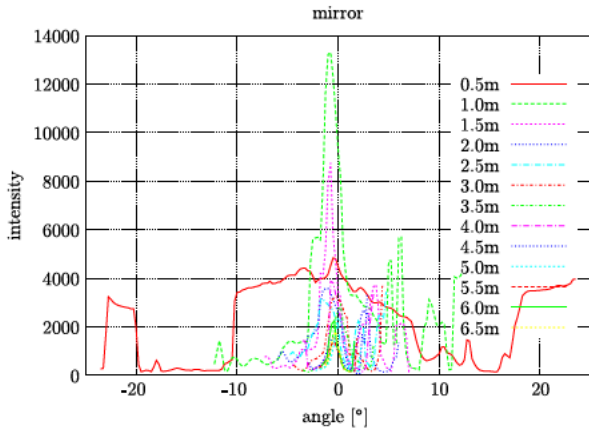


Fig. 12. Measured intensity curves returned from a mirror at different distances.

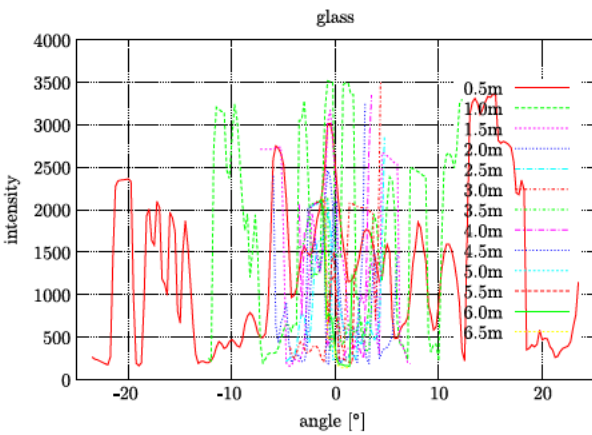


Fig. 13. Measured intensity curves returned from glass at different distances.

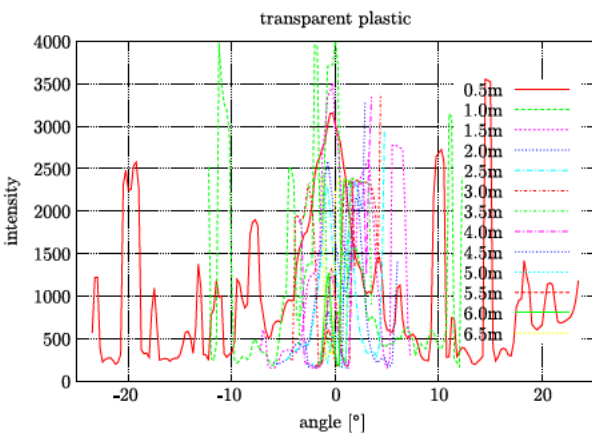


Fig. 14. Measured intensity curves returned from transparent plastic at different distances.

widens with further distance to the source, the intensity spreads amongst a greater area. Nevertheless, there is a similarity between the curves and the proportionality to

$$\frac{1}{s^2}$$

Furthermore, the different intensity ranges relate to the material to be seen.

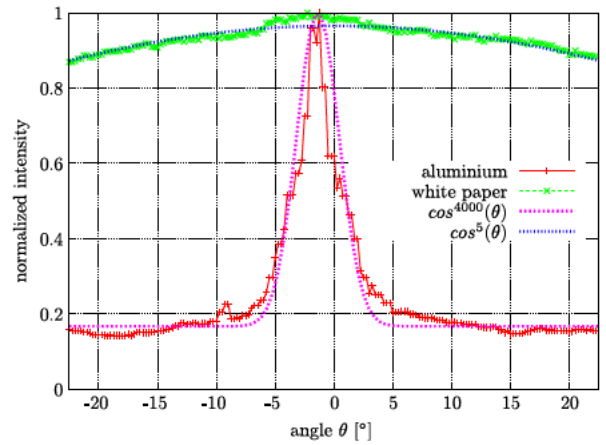


Fig. 15. Fitting $\cos^n \theta$ to white paper and aluminium at $s = 0.5$ m.

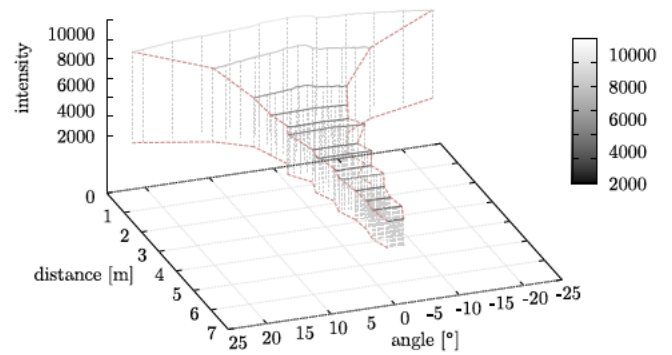


Fig. 16. Intensity characteristic of white paper depending on distance and angle.

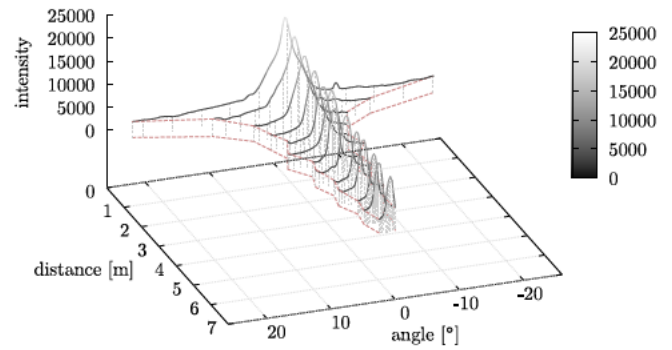


Fig. 17. Intensity characteristic of aluminium depending on distance and angle.

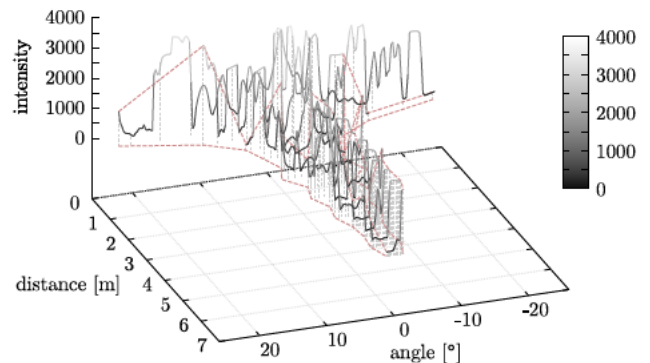


Fig. 18. Intensity characteristic of glass depending on distance and angle.

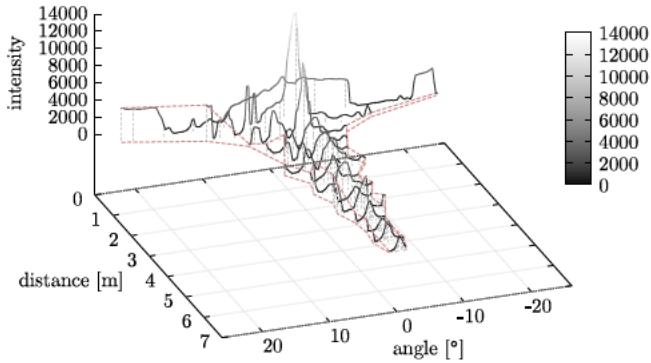


Fig. 19. Intensity characteristic of a mirror depending on distance and angle.

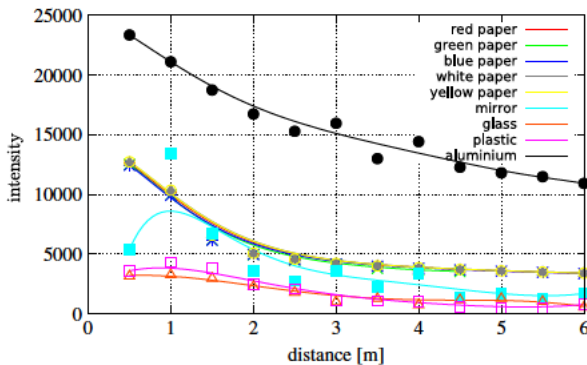


Fig. 20. Intensity characteristic in dependency of distance for different materials.

4.3. Experiment 3: Drive-by scenario

As described previously, the measurement result of a point located on a transparent or specular reflective object depends on the incident angle. Therefore, it is important to bypass such an object to guarantee it being seen from the right perspective. This is why, the third experiment was conducted with the objective of analysing the characteristics of the previously examined materials in the context of a drive-by scenario, cf. Fig. 21. The incident angle between the scanner and a particular sample varies when passing by the object. Hence, the resulting scan history is reprocessed by the post-filter. The experiment simulates a real-world scenario in which a scanner is mounted on a mobile robot. After discovering a lack of information at the sample segment along the wall, the scanner continues to move parallel to the wall till the end of the track. Ideally, the device should have collected enough data to deduce the properties of the examined wall segment once it had entirely passed by it.

To this end, the track used in the second experiment was placed in the first of two aisles, aligned in parallel to its walls. The distances d_{obj} and d_w to the left and right of the track differed deliberately to facilitate the retrospective correlation of the recorded signal intensities to the respective wall. Both aisles were confined in and separated by opaque canvases of vertically mounted facsimile paper. The two mutually obscured aisles are interconnected via an opening that housed the same sample mount already used in the second experiment.

While being slowly towed along the trail by a DC motor with a constant velocity v in the first aisle, thereby covering the track segment s , the distance and incident angle of the scanner changed gradually in relation to the mounted sample b .

$$v_{\text{laser}} \approx \frac{0.278 \text{ m}}{77.36 \text{ s}} = 0.0036 \frac{\text{m}}{\text{s}}. \quad (6)$$

It is understood that the measurements between different samples were not synchronized, since there was no ground truth.

Similar to the second experiment, the angle between the incoming laser beam and the surface normal vector (of the examined object) was compared between the scans. This was done during the side-by-side motion of the robot, in particular, starting from the pose where the beam had a large angle of incidence, to finish at the position where the incidence was perpendicular. This allowed the experimenters to reproduce the intensity change beyond the complete viewing range.

The intensity's absolute value re-increased once the scanner had passed by the sample mount, respectively. In reference to the second experiment, the measurements of the signal echoes were recorded for object samples made of paper with various shades of colours, aluminium, mirror, transparent plastic, and glass, cf. Fig. 7c.

In the case of the paper sample, a material with opaque, mostly diffuse, and non-specular surface characteristics, cf. Fig. 9, the mounted sample served the purpose of a mere variant of the surface characteristics of the surrounding environment, as far as differences regarding the intensity of the respective echoes could be determined. Similar to the mirror case, the sample was used as a reflective material to model the intensity characteristics of the object, as such intensity characteristics change significantly depending on the beam's angle of incidence. It revealed varying intensities regarding its environment in the form of its second echo, cf. Fig. 26.

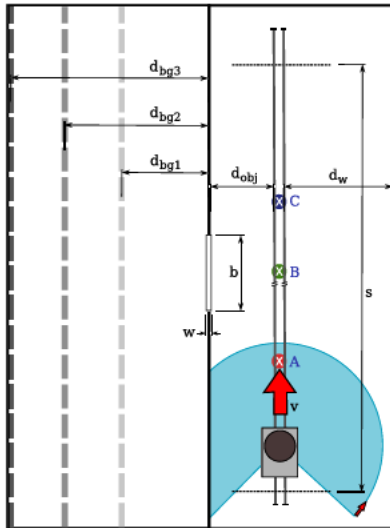
The geometry of the second aisle was varied by setting its width d_{bg_i} to three distinctive distances ($d_{bg_i} \in \{50, 110, 160\}$ cm) and recorded the impact on the intensity of the reflected signal respectively. By doing so, they modelled three specific scenarios to find a correlation between the size of the space behind the transparent opening and the progression of the second echo as the scanner passed by the sample. The confining walls of the second aisle were invariably made of the same paper canvas also used in the first aisle. This was done to avoid interferences caused by inter-reflection that might have complicated the interpretation of the echo.

4.3.1. Extracts of intensity curves

While reviewing the intensity curves of all scans it was difficult to see the progression. Figs. 23–26 show scans of the four samples at three positions (cf. Fig. 21 Pos. A: before passing the sample, Pos. B: perpendicular to the sample, and Pos. C: after passing the sample).

For glass samples as well as for plastic, the intensities of Echo 2, associated with an object behind, are higher than Echo 1. This is due to the transparency of the sample's surface, when most of the light passes through the surface. As with all other non-transparent surfaces for aluminium (cf. Fig. 25) the intensities of Echo 1 are higher than the intensities of Echo 2. The reason for this is that Echo 1 is the first recorded measurement from a certain point and Echo 2 follows. With transparent objects, most light passes through the object surface. Therefore the object in the background causes a stronger intensity value than the transparent surface itself. Since the transparent object was closer to the scanner, its surface measurement was recorded first, hence, as Echo 1. These circumstances are discussed in more detail in Section 4.3.3.

Moreover, a moving “bump” is visible for glass, plastic and aluminium. This can be seen in Fig. 27. This corresponds to the configuration of the setup as well as the Phong reflection model. Before the scanner passed the sample, i.e., at Location A, the rightmost laser beam hitting the surface had a larger distance than the beam belonging to the leftmost border, cf. Fig. 22. At Pos. B the distances to the leftmost and rightmost measurements were equal. At Pos. C, the tendency in red was in direct contrast to Pos. A since



(a) Schematic overview: Scanner on the track with its three set positions (A, B, and C) to measure. The big red arrow indicates the moving direction of the scanner is moving towards. The small red arrow shows the internal scan direction of the laser beam. Broken lines indicate the three positions of the background.



(b) Hardware setup of Hokuyo UTM-30LX-EW with independent power supply and wireless connection to run on the aisle.

Fig. 21. Setup of Experiment 3. (For interpretation of the references to colour in this figure legend, the reader is referred to the web version of this article.)

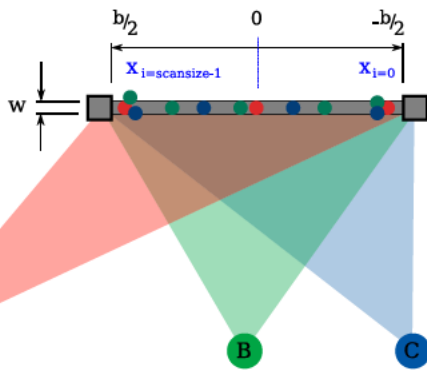


Fig. 22. Location of scan point on the sample, based on the position (Pos. A, Pos. B, and Pos. C) of the laser scanner. (For interpretation of the references to colour in this figure legend, the reader is referred to the web version of this article.)

the leftmost laser beam had the largest distance to the surface, cf. Fig. 22.

Therefore, the “bump” started on the right side (Position A). When passing the sample the bump was moving oppositely to the driving direction. At Position B, the “bump” was located in the middle of the scan. At Position C, the “bump” reached the left side of the scan.

The mirror curves, cf. Fig. 26, show large discontinuities. It is not possible to fit a curve into the scan points. This is similar to the results of Experiment 2, cf. Fig. 12. Moreover, sometimes the intensity values of Echo 1 are sometimes greater than the intensity values of Echo 2, or vice versa.

4.3.2. Intensity curves based on position and incident angle

To illustrate the progression of intensity based on position and incident angle a 3D plot was created. Accordingly, the measurements were filtered. Scans with less than 40 points on sample length b were removed. This is similar to the behaviour of the pre-filter stage of the Mirror Detector. Also, the outer points which

were located next to the edge of the samples were deleted to eliminate outliers. To determine the exact position on the sample plane, each point was recalculated with the assumption that the outer points were at the border of the sample and the points were distributed with equal spacing, cf. Fig. 22. The length x_i was shifted by $-b/2$ to project the origin to the middle of the sample.

$$x_i = \frac{b}{N} \cdot i - \frac{b}{2}, \quad i = [0, N - 1], \quad x_i = \left[-\frac{b}{2}, \frac{b}{2} \right]$$

with $b = 52$ cm is the length of the sample, N is the amount of scan points on the sample, and i is the index of current point (see Fig. 28).

4.3.3. Mean intensity value

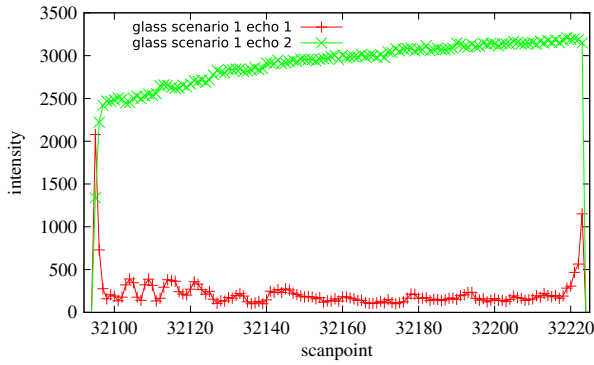
The Mirror Detector includes a pre- and a post-filter module. The post-filter contains the complete history of all scans. Therefore, it seems obvious to consider the trend of the intensity. Figs. 29 and 30 illustrate the arithmetic mean intensity $\hat{I}_{\text{scan_nr}}$ of a scan. Based on the setup the outer test points were ignored. Here, the laser beam might have hit the corners of the sample mount which could have resulted in erroneous measurements.

$$\hat{I}_j = \frac{\sum_{i=1}^N I_i}{N}$$

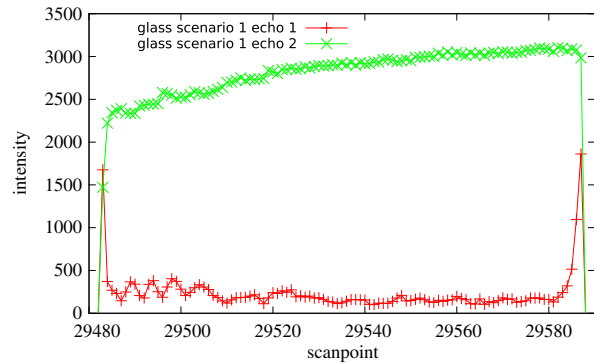
I is the intensity, j is the number of scans of the history L , and N is the amount of points in the scan.

Initially, all curves show a high variation in Echo 1 (red dotted line) as well as in Echo 2 (green solid line). This was due to the fact that the scan data was not preprocessed for this section. Accordingly, scans with only a few scan points on the surface caused a high variation.

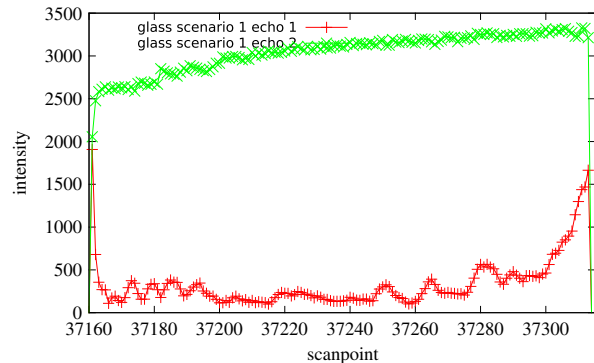
This only happens in the beginning when the incident angle between the incoming laser beam and the surface normal is big. The pre-filter corrects this by dismissing reflective objects with an insufficient number of scan points. Nevertheless, the four graphs illustrate important differences between the characteristics of the materials. The maximum intensity value was estimated at the



(a) Returned intensity at Pos. A before passing the glass front.



(b) Returned intensity at Pos. B when being vertically positioned to the glass front.

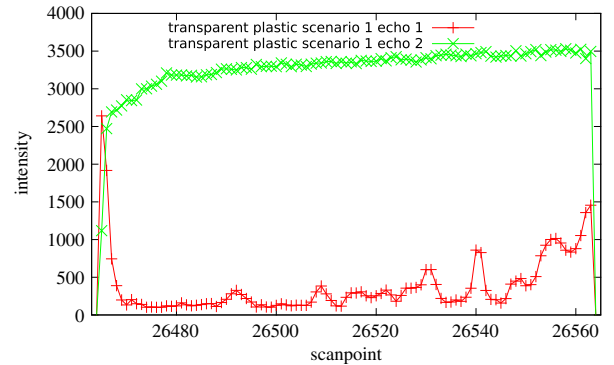


(c) Returned intensity at Pos. C after passing the glass front.

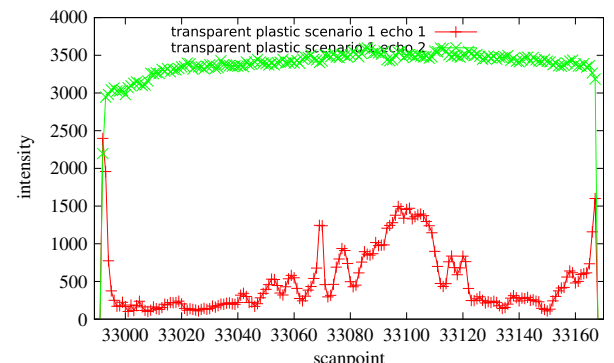
Fig. 23. Intensity values Echo 1 (red) and Echo 2 (green) at different times on glass. (For interpretation of the references to colour in this figure legend, the reader is referred to the web version of this article.)

closest position to the sample. In this case, the laser beam hits the sample surface perpendicularly. The amount of scans varies because all the materials have a different angle sensitivity (cf. Fig. 8 Phong curve Experiment 2).

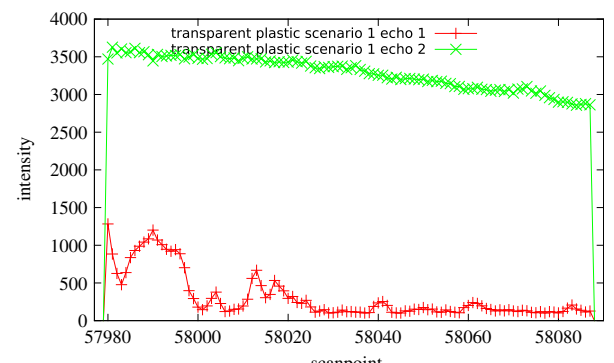
Glass, cf. Fig. 29a, and transparent plastic, cf. Fig. 29b, show similar characteristics. Both graphs show that the intensity of Echo 2 is significantly higher than the intensity of Echo 1. Furthermore, the curve was related to the Phong reflection model for objects with a low n -factor. In the experiment, there was white paper behind the glass surface. In most cases it is unknown where transparent objects are or what kind of surface is behind them. This is why it is important to analyse the intensities of Echo 1 which are associated with the object itself. The intensity values result in a curve with low intensity values and a minimal “bump”.



(a) Returned intensity at Pos. A before passing the plastic front.



(b) Returned intensity at Pos. B when being vertically positioned to the plastic front.



(c) Returned intensity at Pos. C after passing the plastic front.

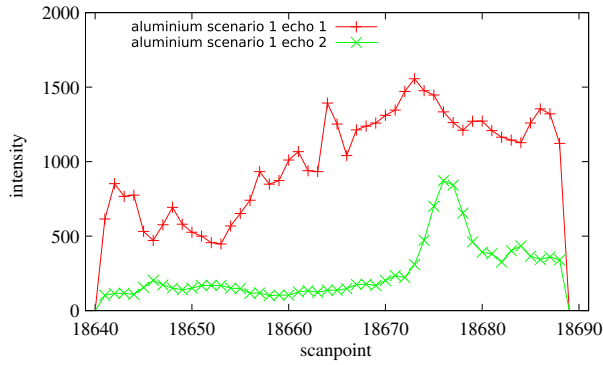
Fig. 24. Intensity values Echo 1 (red) and Echo 2 (green) at different times on transparent plastic. (For interpretation of the references to colour in this figure legend, the reader is referred to the web version of this article.)

The progression of the intensity of Echo 1 and Echo 2 for aluminium, cf. Fig. 30a, differs significantly. Here, the intensities of Echo 1 are greater than the intensities of Echo 2. Moreover, the characteristics of aluminium was seen in both echoes. As previously seen, the curves of the mirror have an overlay of both characteristics.

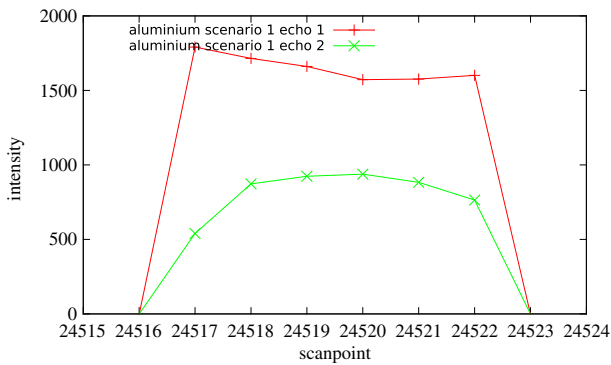
The factor f_{material} between the mean intensity of Echo 1 and Echo 2 is illustrated in Fig. 31.

$$f_{\text{material}} = \frac{\hat{I}_{j_{\text{echo}2}}}{\hat{I}_{j_{\text{echo}1}}} \quad (7)$$

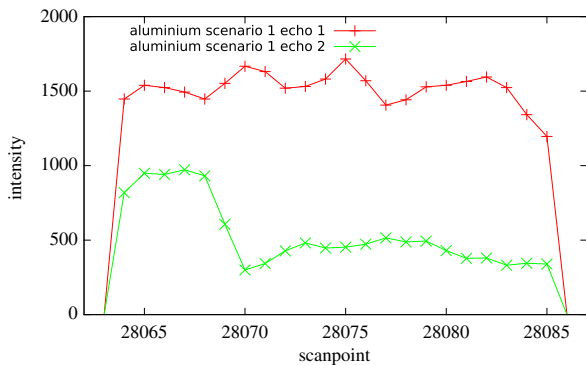
with j is the number of scan of the history L . As previously mentioned for aluminium, the intensity values of Echo 1 are greater than those of Echo 2. Therefore, the factor $f_{\text{aluminium}}$ is lower than



(a) Returned intensity at Pos. A before passing the aluminium front.



(b) Returned intensity at Pos. B when being vertically positioned to the aluminium front.

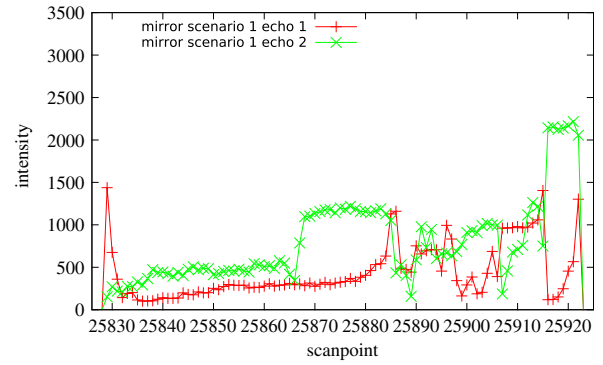


(c) Returned intensity at Pos. C after passing the aluminium front.

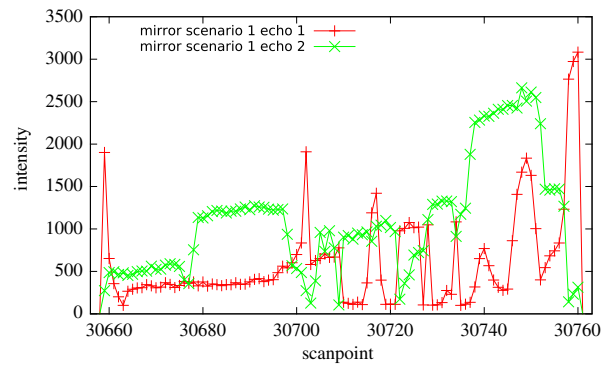
Fig. 25. Intensity values Echo 1 (red) and Echo 2 (green) at different times at aluminium. (For interpretation of the references to colour in this figure legend, the reader is referred to the web version of this article.)

1. For the mirror surface the factor f_{mirror} is ~ 1 and for glass significantly greater than 1. It is worth mentioning that the number of scans varies in the history. This is due to the fact that different materials have different reflective characteristics and therefore different sensibility depending on the angle, as was shown in Section 4.2.1. Therefore, the aluminium sample has fewer detected scan points than the mirror sample. As a result the curves were not “synchronized”. For objects close behind the glass surface (Fig. 32a $\rightarrow d_{\text{bg}1} = 50$ cm) the factor f_{glass} is greater than for an object further away (Fig. 32b $\rightarrow d_{\text{bg}2} = 110$ cm, Fig. 32c $\rightarrow d_{\text{bg}3} = 160$ cm).

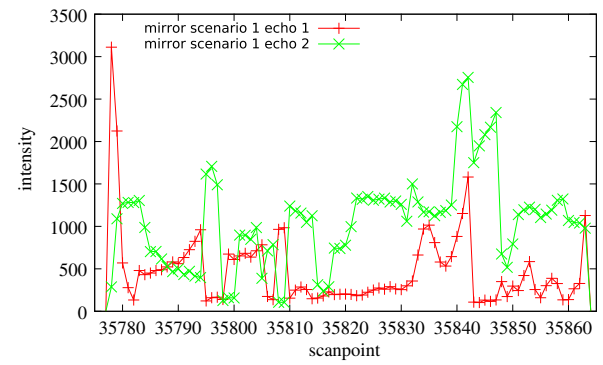
The characteristics of transparent surfaces depend on the object behind it. Fig. 32 illustrates the dependency of white paper behind the glass surface at different distances d_{bg} . On the one hand, the maximum value of the intensity of Echo 2 shrinks, the further the object is placed behind the sample. This corresponds to the results



(a) Returned intensity at Pos. A before passing the mirror front.



(b) Returned intensity at Pos. B when being vertically positioned to the mirror front.



(c) Returned intensity at Pos. C after passing the mirror front.

Fig. 26. Intensity values Echo 1 (red) and Echo 2 (green) at different times at a mirror. (For interpretation of the references to colour in this figure legend, the reader is referred to the web version of this article.)

of distance dependency in Experiment 2 in Section 4.2.2. On the other hand, a “bump” in Echo 1 grows, which was also confirmed in Experiment 2. This leaves no doubt that this effect needs further investigation.

This experiment describes the results of the applied research of Experiment 2 and Experiment 3 implemented in the Reflection Classifier Approach. The Reflection Classifier is an extended version of the Mirror Detector Approach. For this reason the function `identifyReflectionType()` is integrated in the post-filter.

4.3.4. Extension to post-filter

The function `identifyReflectionType()` (cf. Fig. 3) is integrated in the post-filter of the Mirror Detector Approach (cf. Algorithm 2). It discriminates the reflective object according to its type.

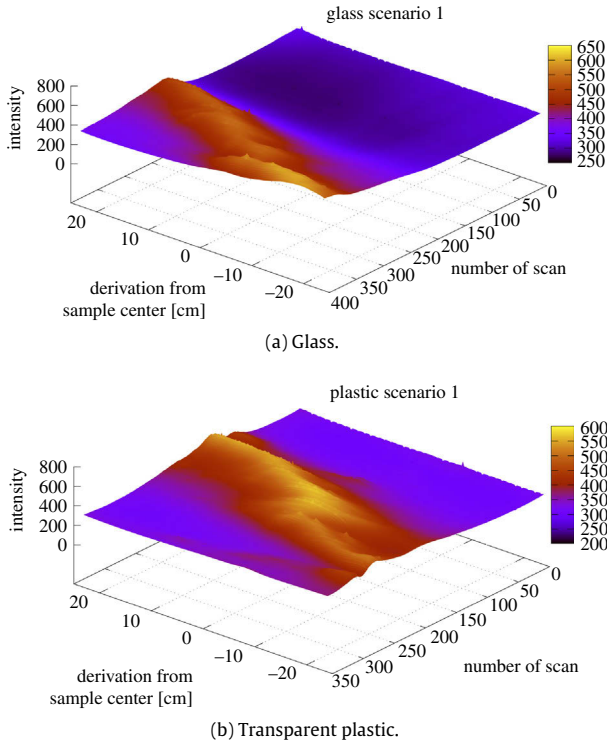


Fig. 27. Echo 1 intensity curve via angle and position of glass and transparent plastic.

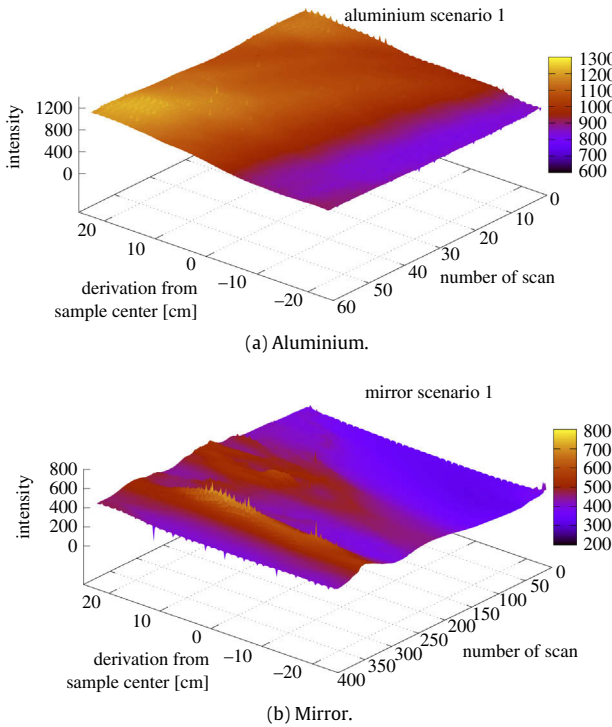


Fig. 28. Echo 1 intensity curve via angle and position of aluminium and a mirror.

For each object O the function scans the masked points of the entire scan history G_{A2} with its length L , if the point is located on its surface or behind it. Subsequently, the object surface is

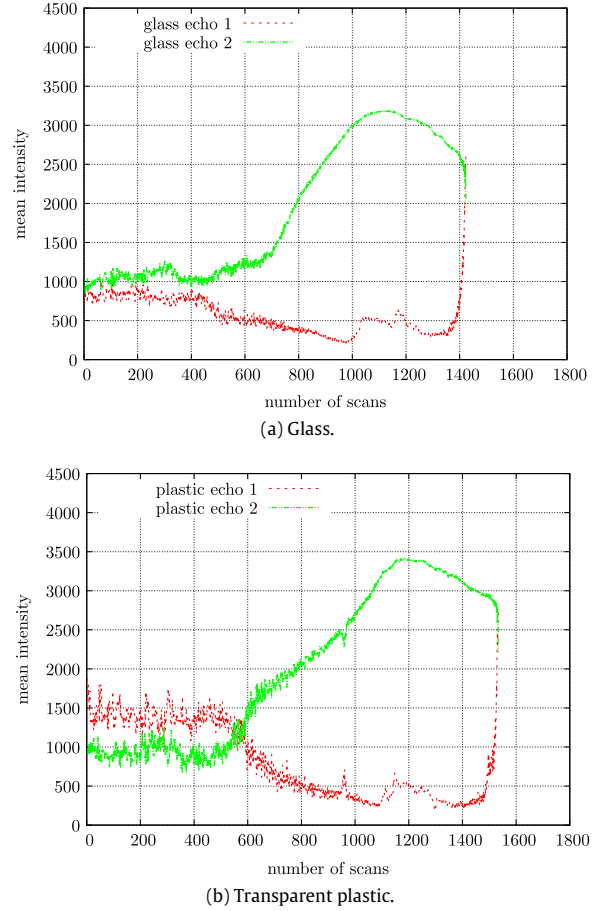


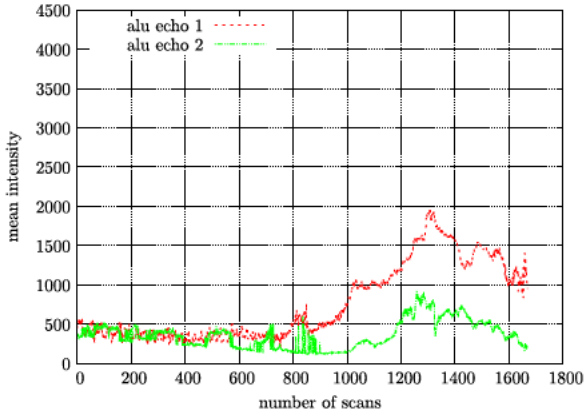
Fig. 29. The mean intensity of Echo 1 (red dotted) and Echo 2 (green solid) per scan for glass and transparent plastic.

identified throughout and across all scans in three steps. Finally, it rates the different identification techniques to result a final object type.

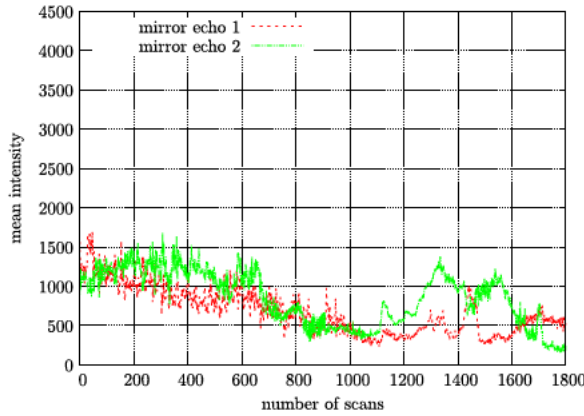
The first function, *checkPhong()*, was implemented in order to accommodate a Phong model curve into the intensity values of each scan. This function was based on the results of Section 4.2.1. The experiment showed that the results were less significant. As already mentioned in Section 4.2.1 only non translucent surfaces can be assimilated to the Phong model. Attempts with glass and plastic were unsuccessful (cf. Figs. 13 and 14). Even for a mirror it is hard to fit the Phong model (cf. Fig. 12).

The second function *checkIntensityFactor()*, builds the mean intensity of the first and the second echo of a single scan and compares them. It runs through all scans and counts “transparent” and “mirror” hits. Finally the object is rated as the amount of the most hits and the function returns the result of this step.

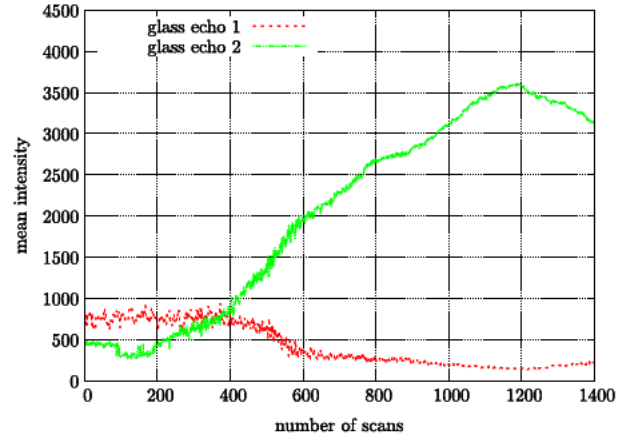
The third function *checkReflectedPoints()* reprojects the points behind the object back to their original locations and searches for an identical object nearby. This function is similar to the idea of Yang [7] and is not directly related to the previous experiments in this study. Even then this is an important method to identify this type of reflection. After the points are reprojected back to their original locations, they are used as a scene while the rest of the scan, the “valid” masked points, are used as a model for the following ICP algorithm. ICP algorithm determines a transformation matrix. If a transformation is found and points to a nearby location, the object for this scan is rated as a mirror. Nearby locations are determined as being close to the reprojected location



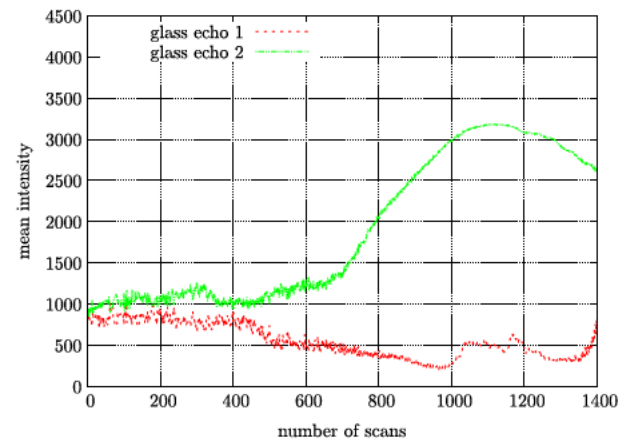
(a) Aluminium.



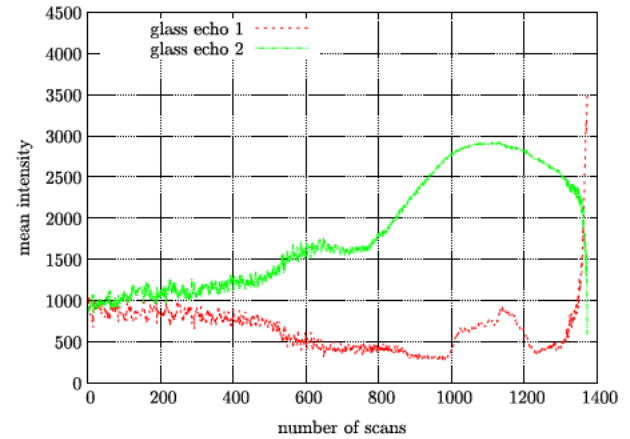
(b) Mirror.



(a) Glass with object behind $d_{bg1} = 50$ cm.



(b) Glass with object behind $d_{bg2} = 110$ cm.



(c) Glass with object behind $d_{bg3} = 160$ cm.

Fig. 30. The mean intensity of Echo 1 (red dotted) and Echo 2 (green solid) per scan for aluminium and a mirror.

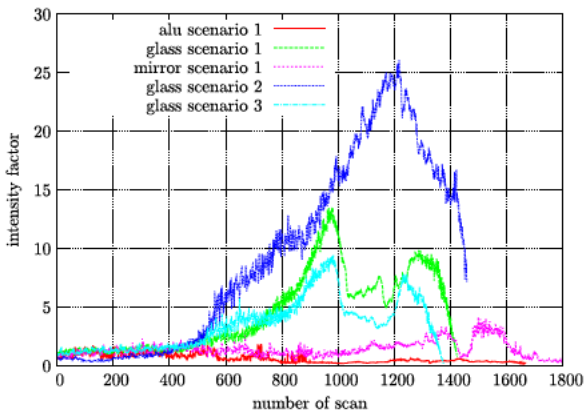


Fig. 31. Factor $f_{material}$ of the mean intensity of Echo 2 and Echo 1 for different materials.

and are identified by adding a threshold for distance and angle. A transformation is needed since there are too many uncertainties in the model and the measurements. Therefore the reprojected points are assumed to be at an offset angle and position. The ICP algorithm removes this error. In the end the function returns an object type based on the amount of valid transformation (mirror) versus invalid transformation (transparent).

In the end, the function `rateResults()` compares the three results and returns a final rating for the object. Reliability is assigned a confidence value for each obtained result. Final function results are

Fig. 32. The mean intensity of Echo 1 (red dotted) and Echo 2 (green solid) per scan for glass with a white object at different distances behind the glass.

then given confidently based on this reliability scale. Following, the history G_{A2} of all scans is searched to remask the points according to their object type. This results in the history G_{A3} .

4.3.5. Results of experiment 4

Fig. 33 shows a refined map of Experiment 1 from the Mirror Detector (cf. Fig. 33a) and a refined map of the Material Classifier (cf. Fig. 33b). The surfaces of the mirror and the glass surface are

all materials, a long term interpretation provided us with more detailed insight.

To identify materials, it was not possible to rely on a single principle as there were too many unknown factors. That is why the discrimination function was determined by considering the following factors:

- fitting $\cos^n \theta$ to a normalization of Echo 1 and Echo 2
- observe changes of the n -factor over time
- rate the magnitude and progression of factor f_{material}
- re-project the affected points back to search for a transformation matrix to the rest of the scan.

The final experiment showed the applied discrimination and the improvement for SLAM. Furthermore, non-planar surfaces need to be modelled to cover a greater field of reflective and transparent objects.

Therefore future work will concentrate on transparent object behaviour with different background circumstances. This will result in a better model to identify reflection types.

Based on the knowledge of the surface material it is possible to process the points located behind a surface. It was the aim to use these points as well for mapping after they had been reprojected back to their original locations. Further it is necessary to reduce the mapping modules. It is desired to use only a single map. Working with two maps carries two main drawbacks. On the one hand it needs more calculation power and storage to process the data. On the other hand the robot relies on the preliminary map which is not free of all reflective influences. Therefore the robot does not process the data of the refined map at all. One idea to overcome these drawbacks is to merge the two maps, e.g., each time after the post filter finished.

This will help to archive the environment, such as mapping modern glass galleries or historic buildings. Castles and palaces are full of reflective and transparent objects, e.g., chandeliers, golden artwork, or mirror cabinets. The aim is to support robust localization and mapping in such challenging areas.

References

- [1] I.S. Department, *World Robotics - Service Robots 2013*, International Federation of Robotics (IFR), 2013/2014 doi:ISBN:978-3-8163-0657-3.
- [2] R. Koch, S. May, P. Koch, M. Kühn, A. Nüchter, Detection of specular reflections in range measurements for faultless robotic SLAM, in: L.P. Reis, A.P. Moreira, P.U. Lima, L. Montano, V. Muñoz-Martinez (Eds.), *Robot 2015: Second Iberian Robotics Conference*, in: *Advances in Intelligent Systems and Computing*, vol. 417, Springer International Publishing, 2016, pp. 133–145. http://dx.doi.org/10.1007/978-3-319-27146-0_11.
- [3] M. Tsardoulias, ROS CRSM SLAM package, 2015. http://wiki.ros.org/crsm_slam. Online (Accessed 25 November 2015).
- [4] S. Kohlbrecher, J. Meyer, ROS Hector SLAM package, 2015. http://wiki.ros.org/hector_slam. Online (Accessed 25 November 2015).
- [5] P. Koch, S. May, M. Kühn, ROS TSD SLAM package, 2015. http://wiki.ros.org/ohm_tsd_slam. Online (Accessed 25 November 2015).
- [6] S.-W. Yang, C.-C. Wang, Dealing with laser scanner failure: Mirrors and windows, in: *IEEE International Conference on Robotics and Automation ICRA*, 2008, pp. 3009–3015.
- [7] S.-W. Yang, C.-C. Wang, On solving mirror reflection in LIDAR sensing, *IEEE/ASME Trans. Mechatronics* 16 (2) (2011) 255–265. <http://dx.doi.org/10.1109/TMECH.2010.2040113>.
- [8] P. Foster, Z. Sun, J.J. Park, B. Kuipers, VisAGGE: Visible angle grid for glass environments, in: *Robotics and Automation (ICRA)*, 2013 IEEE International Conference on, 2013, pp. 2213–2220. <http://dx.doi.org/10.1109/ICRA.2013.6630875>.
- [9] A. Tatoglu, K. Pochiraju, Point cloud segmentation with LIDAR reflection intensity behavior, in: *Robotics and Automation (ICRA)*, 2012 IEEE International Conference on, 2012, pp. 786–790. <http://dx.doi.org/10.1109/ICRA.2012.6225224>.
- [10] J.F. Blinn, Models of light reflection for computer synthesized pictures, in: *Proceedings of the 4th Annual Conference on Computer Graphics and Interactive Techniques*, in: *SIGGRAPH'77*, ACM, New York, NY, USA, 1977, pp. 192–198. <http://dx.doi.org/10.1145/563858.563893>.
- [11] K.E. Torrance, E.M. Sparrow, Theory for off-specular reflection from roughened surfaces, *J. Opt. Soc. Am.* 57 (9) (1967) 1105–1112. <http://dx.doi.org/10.1364/JOSA.57.001105>. URL <http://www.opticsinfobase.org/abstract.cfm?URI=josa-57-9-1105>.
- [12] P. Beckmann, A. Spizzichino, *The Scattering of Electromagnetic Waves from Rough Surfaces*, Pergamon Press, 1963. URL http://books.google.de/books/about/The_scattering_of_electromagnetic_waves.html?id=QBEIAQAAIAJ&redir_esc=y.
- [13] H. Yoshitaka, K. Hirohiko, O. Akihisa, Y. Shin'ichi, Mobile robot localization and mapping by scan matching using laser reflection intensity of the SOKUIKI sensor, in: *IEEE Industrial Electronics, IECON 2006 - 32nd Annual Conference on*, 2006, pp. 3018–3023. <http://dx.doi.org/10.1109/IECON.2006.347701>.
- [14] H. Yoshitaka, K. Hirohiko, O. Akihisa, Y. Shin'ichi, Map building for mobile robots using a SOKUIKI sensor-robust scan matching using laser reflection intensity, in: *SICE-ICASE, 2006. International Joint Conference*, 2006, pp. 5951–5956. <http://dx.doi.org/10.1109/SICE.2006.315836>.
- [15] P. Besl, N. McKay, A method for registration of 3-D shapes, *IEEE Transactions on Pattern Analysis and Machine Intelligence* 14 (1992) 239–256. <http://doi.ieeecomputersociety.org/10.1109/34.121791>.
- [16] P. Koch, S. May, M. Schmidpeter, M. Kühn, J. Martin, C. Pfitzner, C. Merkl, M. Fees, R. Koch, A. Nüchter, Multi-robot localization and mapping based on signed distance functions, in: *Autonomous Robot Systems and Competitions (ICARSC)*, 2015 IEEE International Conference on, 2015. <http://robotica2015.utad.pt/en/ICARSC>.
- [17] A. Watt, *3D Computer Graphics*, Addison Wesley, 2000.



Rainer Koch received his diploma (power engineering and system control) in 2007 and his Master's degree (electrical and mechatronical systems) in 2010 from the Georg-Simon Ohm University of Applied Science in Nuremberg. Between 2007 and 2011 he was working as a research assistant at the Institute for Power Electronics ELSYS at the Georg-Simon Ohm University of Applied Science. Since 2011 he is a Ph.D. student at the autonomous robotics team at the Technische Hochschule Nürnberg Georg-Simon Ohm. His research interests include sensor and data processing for 2D and 3D perception of

mobile robots.



Stefan May received a diploma (electrical engineering) in 2000 and a Master's degree (software engineering) in 2004 from the Georg-Simon Ohm University of Applied Science in Nuremberg. In 2009 he received his Ph.D. in computer vision from the University in Osnabrueck. Between 2002 and 2009 he was working in the context of test systems for automotive electronics at Audi and 3D vision for robotic perception at Fraunhofer IAIS in Germany and INRIA in France. Since 2010, he is professor for Automation and Mechatronics at the Technische Hochschule Nürnberg Georg-Simon Ohm. His research interests include sensor and data processing for 3D perception of mobile robots.

and data processing for 3D perception of mobile robots.



Patrick Murmann works as a research assistant for the autonomous robotics team at Technische Hochschule Georg-Simon Ohm in Nuremberg where his main responsibilities lie with semantic imaging. He received his M.Sc. at the department of computer science.



Andreas Nüchter is a professor for Computer Science at the University of Würzburg. Between 2009 and 2013 he had a professorship at the Jacobs University in Bremen. Past affiliations were with the Fraunhofer Institute for Autonomous Intelligent Systems (AIS, Sankt Augustin) and University of Bonn, from which he received the diploma degree in computer science in 2002 (best paper award by the German Society of Informatics (GI) for his thesis). He holds a doctorate degree (Dr. rer. nat) from University of Bonn. His research interests include reliable robot control, 3D environment mapping, 3D vision, and laser scanning technologies, resulting in fast 3D scan matching algorithms that enable robots to map their environment in 3D using six degrees of freedom poses. The capabilities of these robotic SLAM approaches were demonstrated at RoboCup Rescue competitions, ELROB and several other events. He is a member of the GI and the IEEE.